Research Article

Design of iron-ion-doped pomelo peel biochar composites towards removal of organic pollutants

Dong-Xu Liu[1] · Juan Mu[1] · Qian Yao[1] · Yang Bai[1] · Fei Qian[1] · Fang Liang[1] · Fa-Nian Shi[1] · Jun Gao[2]

Abstract
After treated with saturated iron(II) chloride water solution at pH ~ 2, pomelo peel was used as precursor for preparation of 3 biochar composites (named CFe1, CFe2 and CFe3, accordingly) via hydrothermal treatment and followed calcination in air, respectively. The as-obtained C/Fe biochar composites were studied with PXRD, SEM, EDS, UV–visible spectroscopy and specific surface area device to analyze their phase, morphology, composition, capacity for light absorption and specific surface area. Furthermore, the adsorption and photocatalytic performances of the 3 biochar composites on rhodamine B (RhB) water solution were investigated. The experimental results show that the hydrothermal pomelo peel biochar composites have better adsorption performance in degrading RhB than that obtained from calcining pomelo peel in air, but opposite for the photocatalytic performance. The removal of imidacloprid (a pesticide) from water via CFe1 was also studied.

Keywords Pomelo peel · Biochar · Composite · Rhodamine B · Imidacloprid · Adsorption · Photocatalysis

1 Introduction

With the development of modern industry, the pollution of organic wastes to water system is getting worse. Organic pollutants in water can directly or indirectly poison aquatic organisms and humans [1–5], accelerate the destruction and degradation of the ecological environment, restrict the development of industry and cause economic losses [6–8]. Therefore, it is of crucial importance to seek efficient and inexpensive technologies for waste water treatment. Currently, organic pollutants treatment methods mainly include physical methods (adsorption, membrane separation, etc.), chemical methods (photocatalysis, chemical oxidation, etc.) and biological methods [9–12]. Since plant residues have high adsorption capacity for organic pollutants, and they are easily modified into adsorbents with high adsorption capacity, more and more researches have been conducted on the removal of organic pollutants by biomass materials [13–19]. Although a variety of adsorbent materials exhibit superior adsorption performance, the treatment of saturated adsorbent materials is challenged and secondary contamination is likely to occur [20, 21]. Photocatalytic degradation technology, as an efficient pollutant treatment technology, has many advantages, mainly including high processing efficiency, no secondary pollution, simple operation and high removal efficiency for low concentration and refractory organic pollutants compared with traditional waste water treatment [22–24], however, photocatalysts that have been developed have a narrow response range to sunlight and a problem of poor stability [25–28]. Therefore, we try to combine the adsorption and degradation technologies to prepare several new iron-ion-contained biochar composites (CFe1, CFe2 and CFe3) that possess both the ability effectively to adsorb

✉ Fa-Nian Shi, shifn@sut.edu.cn; Dong-Xu Liu, grace.dxl@foxmail.com; Juan Mu, jmu.cx@foxmail.com; Qian Yao, april.qy@foxmail.com; Yang Bai, andy.qd@foxmail.com; Fei Qian, qianfei0987@foxmail.com; Fang Liang, liangfang@sinochem.com; Jun Gao, gaojchen@public.qd.sd.cn | [1]School of Science, Shenyang University of Technology, Shenyang 110870, China. [2]College of Chemical and Environmental Engineering, Shandong University of Science and Technology, Qingdao 266590, China.

SN Applied Sciences (2019) 1:184 | https://doi.org/10.1007/s42452-019-0188-y

Received: 3 December 2018 / Accepted: 18 January 2019 / Published online: 29 January 2019

and catalytically to degrade organic pollutants under the irradiation of visible sunlight.

2 Materials and methods

2.1 Materials and instruments

Pomelo peel was dried naturally before use. Iron(II) chloride tetrahydrate ($FeCl_2{\cdot}4H_2O$, 99.7%, Damao chemical reagent factory in Tianjin), hydrochloric acid (34–37%), Rhodamine B ($C_{28}H_{31}ClN_2O_3$, Damao chemical reagent factory in Tianjin), Imidacloprid ($C_9H_{10}ClN_5O_2$). Powder X-ray Diffraction Apparatus (Mini Flex600, Japan Science Company), scanning electron microscope (Phenom ProX, Fina Corporation), specific surface area and pore size analyzer (JW-BK122W), UV–visible spectrophotometer (TU-1950, Cape Analysis).

2.2 Pomelo peel modification

The pomelo peel was modified by one-step modification and two-step modification, respectively [29, 30].

2.2.1 Two-step modification

1.74 g of dried pomelo peel was immersed in a saturated iron(II) chloride solution with pH ~ 2 for 7 days, then placed in a 100 ml reaction vessel together with 50 ml of the saturated iron(II) chloride solution to be hydrothermally treated at 200 °C for 5 h in an electric blast drying oven, then naturally cooled to room temperature, filtered, and the solid residue was dried at 100 °C and 1.17 g of black biochar composite was obtained (namely CFe1, yield ~ 67.2% based on pomelo peel).

Another 2.73 g of pomelo peel was soaked in a saturated iron(II) chloride solution with pH ~ 2 for 7 days, then loaded into a crucible and calcined at 300 °C for 2 h in a muffle furnace under air atmosphere, then cooled to room temperature in the furnace, 2.47 g of brown biochar composite was harvested (namely CFe2, yield ~ 90.5% based on pomelo peel).

2.2.2 One-step modification

2.54 g of dried pomelo peel together with 50 ml of a saturated iron(II) chloride solution with pH ~ 2 were placed in a 100 ml reaction vessel to react in an electric blast drying oven at 200 °C for 5 h, then naturally cooled to room temperature, filtered, the solid residue was dried at 100 °C and 2.87 g of black biochar composite was obtained (namely CFe3, yield ~ 113% based on pomelo peel).

2.3 Characterization techniques

The phases of the 3 biochar composites were identified using powder X-ray diffraction (PXRD) on a MiniFlex600 diffractometer (40 kV, 15 mA) with Cu Kα (λ = 0.15405 Å) in a 2θ range from 5° to 80°. The morphologies, contents and elemental distribution of the 3 samples were observed using a scanning electronic microscope (SEM) and an energy dispersive spectrometer (EDS) of Phenom proX with CeB_6 filament, working at 10 kV. The SEM samples were coated by gold on a SBC-12 ion sputtering instrument. Specific surface area and pore size analyzer (JW-BK122W) was used to analyze the specific surface area of the samples. The UV–visible diffuse reflection spectra were performed on a UV–Vis spectrophotometer (TU-1950, Cape Analysis) equipped with an integrating sphere. The UV–visible diffuse reflection data was converted to the following Kubelka–Munk function (F(R)). Tauc plots take $h\nu$ as abscissa and $(F(R){\cdot}h\nu)^{1/2}$ as ordinate.

$$h\nu = \frac{1240}{\lambda}$$

$$F(R) = \frac{(1-R)^2}{2R}$$

2.4 Adsorption and photocatalysis

2.4.1 Preparation of target degradation product

0.020 g of RhB powder together with 1000 ml distilled water were loaded into a cleaned 1000 ml volumetric flask to prepare RhB solution with the concentration of 20 mg/l for use.

2.4.2 Photocatalysis methods

Photocatalytic experiments using the 3 composites in sequence were performed under the same conditions. Therefore, here the experiment with CFe1 is taken as an example and is described in detail. 0.1 g of CFe1 (CFe2: 0.1 g; CFe3: 0.1 g in other cases) was added into 100 ml RhB solution with a concentration of 20 mg/l together with a magnetite bar, and the adsorption performance was conducted in a dark environment (dark reaction) with stirring for 0.5 h. Then the light source system was turned on, the photocatalytic performance started (light reaction), the magnetic stirrer kept stirring during light reaction, and the reaction temperature was kept at room temperature (~ 25 °C) by cooling water circulation, the xenon light source current was 16 A, the light source was visible light, wavelength range of 350–780 nm. Each

0.25 h during the reaction, a small amount of the solution was taken from the degrading tank, centrifuged, and the supernatant was taken and measured by UV–visible spectroscopy.

3 Results and discussion

3.1 Different preparation for iron-ion-doped biochar composites

The modified substance is a strong acidic ferrous chloride solution, which can improve the surface acidity and pore structure of the biochar. It is expected that CFe1 obtained by immersion activation and hydrothermal treatment will have better adsorption performance because prolonged immersion, high temperature and high pressure environment are favorable for the formation of pore structure; since calcination in air atmosphere is easy to form oxides, it is possible the pore structure will be blocked, the specific surface area of CFe2 will be small, which will affect its adsorption performance, but the photocatalytic performance of the resulting semiconductor oxide may be better than those obtained by hydrothermal treatment; the adsorption performance of CFe3 should be in the middle among the 3 biochar composites. The above reasonable inferences and predictions have also been verified through subsequent characterizations and experiments.

3.2 Morphology and composition

Figure 1a–c shows the images of CFe1, CFe2, CFe3 on the scanning electron microscopy (SEM). The surface of CFe1 is rough and porous with uniform pore size and a great deal of adsorption sites. The above characteristics are beneficial to the adsorption of pollutants. The surface of CFe2 is also rough and porous, but the pore structure is not as uniform as CFe1. The surface porosity of CFe3 is less but larger. These observed phenomena are consistent with the data of the specific surface area. Thus we can infer that hydrothermal treatment is more conducive to the formation of porous structures because of high pressure, and the adsorption and photocatalytic performances of CFe1 and CFe3 are better than that of CFe2.

Figure 1d–f shows the energy dispersive spectrometer analyses (EDS) of CFe1, CFe2 and CFe3. The contents of the contained elements were quantitatively analyzed. It can be observed from the figure that the surface of the samples mainly contains C, Fe, Cl and O elements. C and O are mainly related to the composition of pomelo peel, whereas Fe and Cl are mainly the result of modification.

3.3 Specific surface area analysis

The specific surface area is one of the important factors affecting the adsorption and photocatalytic performance. The specific surface areas of the 3 biochar composites are 35.80 m^2/g, 15.87 m^2/g and 32.56 m^2/g, respectively. The specific surface area of CFe1 is the largest, which is mainly the result of acidic ferrous chloride activation and hydrothermal carbonization. It is consistent with the results observed in the SEM photograph (Fig. 1).

3.4 Powder X-ray diffraction analysis

Powder X-ray diffraction patterns of CFe1, CFe2 and CFe3 are shown in Fig. 2. Compared with the standard cards (Serial number of the standard cards: 72-0268, 79-1741 and 72-0268), it was found that the main peaks of CFe1 and CFe3 are ferrous chloride dihydrate, the main peak of CFe3 is di-iron trioxide (Fe_2O_3), whose grain size is about 0.45 nm. These results demonstrate that $FeCl_2{\cdot}2H_2O$ is dispersed as a main component to CFe1 and CFe3 biochar composites treated under hydrothermal conditions, while Fe_2O_3 is employed as a main component to diffuse to CFe2 biochar composite during sintered in air.

3.5 UV–visible absorption spectroscopy analysis

Figure 3 shows Tauc plots and the UV–visible absorption spectra of CFe1, CFe2, CFe3. From the Tauc curves, we can see that the forbidden band widths of the 3 biochar composites are 3.0 eV for CFe1, 2.0 eV for CFe2 and 1.8 eV for CFe3, respectively. Therefore, it was found that CFe2 contains α-Fe_2O_3. Nano-sized α-Fe_2O_3 is widely used in chemical catalysis and photocatalytic environmental treatment because of its large specific surface area, small particle size, more stable chemical properties, and high catalytic activity [31, 32]. Theoretically, the reduction of the forbidden band width is conducive to the adsorption of light, thus leading to higher photocatalytic activity.

By comparing the UV–visible absorption spectra of the 3 biochar composites, we find for CFe1, the light absorption is the weakest in the whole region. In contrast, CFe2 and CFe3 have relatively stronger light absorption, CFe3 has stable absorption throughout the region and CFe2 absorbs weakly in the range of 550–700 nm. This is in accordance with the result of the forbidden band width, therefore, CFe2 and CFe3 may have higher photocatalytic activity, too.

3.6 Adsorption and photocatalytic analysis

Figure 4 compares the degradation efficiency of RhB with the 3 biochar composites (CFe1, CFe2 and CFe3) as

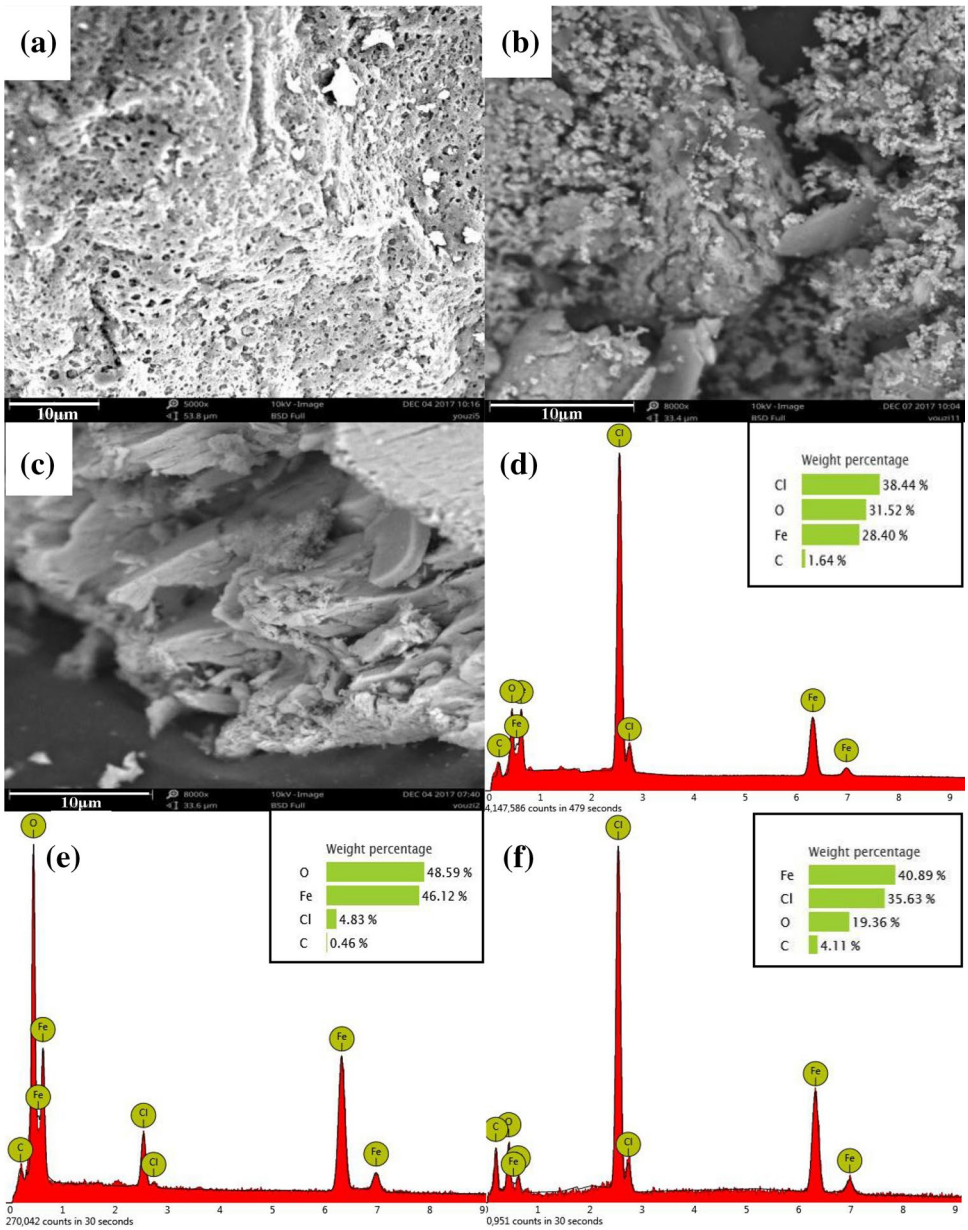

Fig. 1 **a**–**c** SEM images of CFe1 × 5000, CFe2 × 8000, CFe3 × 8000; **d**–**f** EDS spectra of CFe1, CFe2, CFe3 (inset: content of different elements)

photocatalyst under UV–visible light. As the figure shows, the adsorption of the 3 biochar composites in 30 min under dark reaction from strong to weak is CFe1 > CFe3 > CFe2 (CFe1: 79.7%; CFe2: 35.5%; CFe3: 54.0%). This may be due to the fact that the surface of CFe1 is coarse and porous (Fig. 1a), with the largest specific surface area and the most uniform pore size. However, the order of photodegradation rate in the photoreaction phase is CFe2 > CFe3 > CFe1 (CFe1: 12.5%; CFe2: 53.6%; CFe3: 33.9%). This is mainly attributed to the presence of α-Fe_2O_3 in CFe2. In general, the degradation capacities of the 3 biochar composites are almost equal in 105 min (CFe1: 92.2%; CFe2: 89.1%; CFe3: 87.9%). Three products follow the law of fast-and-slow during adsorption and photocatalytic process.

We weighed 0.20 g of CFe1 and CFe2 for cyclic testing, and found that their adsorption and photocatalytic effects were greatly reduced in the cycle test. The loss of photocatalyst is very serious. For example, CFe1 only had 5% (in weight) left after one cycle, and CFe2 25%, which may be attributed to operation and recycling largely, but the loss for CFe1 is more serious, so it is speculated that the $FeCl_2 \cdot 2H_2O$ in CFe1 may be dissolved or changed during the photocatalytic experiment, and powder X-ray diffraction patterns have proved the change, Therefore, we can figure out that CFe2 is more stable than CFe1.

In addition, because of the excellent behavior of RhB photocatalysis, CFe1 was selected for degradation experiment of a pesticide residue. A 0.10 g of CFe1 was weighed

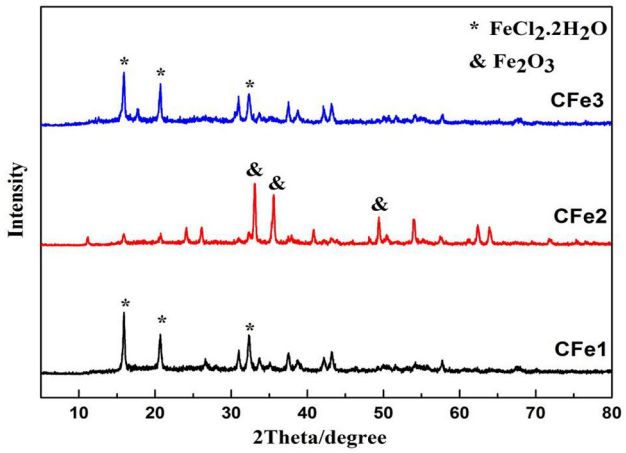

Fig. 2 Powder X-ray diffraction patterns of CFe1, CFe2, CFe3

for adsorption and photocatalytic test of imidacloprid with the concentration of 10 mg/l. The adsorption was 18.7% in weight within 30 min, and the photocatalytic degradation in 90 min was 13.6% under irradiation of visible light. It can be concluded that CFe1 is selective for adsorption and degradation of different pollutants.

We also compared the pomelo peel biochar obtained by direct hydrothermal treatment and calcination without doping metal ion for modification [33]. And it turns out that the modified biochar composites have much better performance on removal of organic pollutants from water. Thus, the modification of biochar materials facilitates the adsorption and photocatalytic degradation of aqueous solutions of organic pollutants.

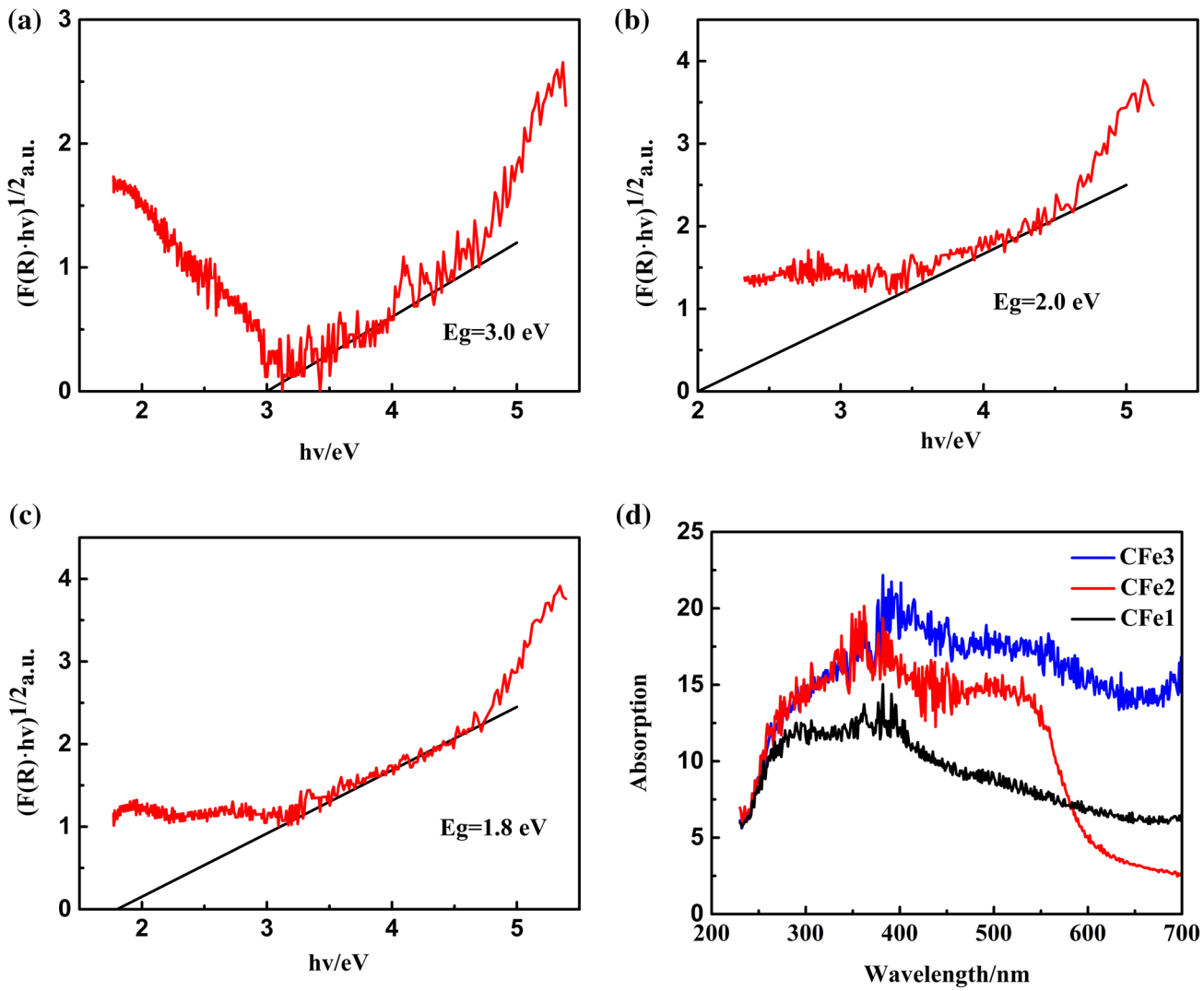

Fig. 3 Tauc plots for CFe1 (**a**), CFe2 (**b**), CFe3 (**c**) and UV–visible absorption spectra of CFe1, CFe2, CFe3 (**d**)

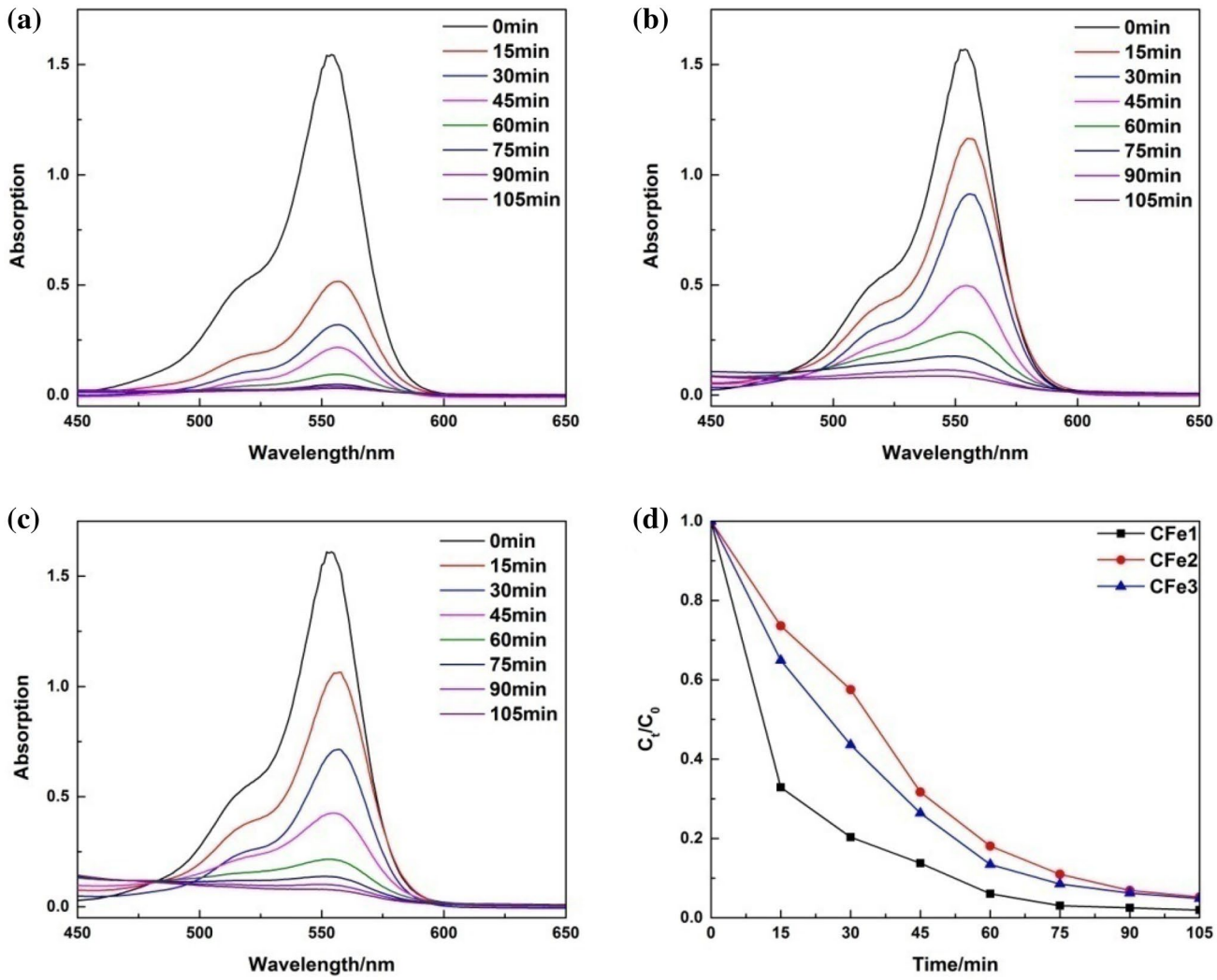

Fig. 4 UV–visible absorption spectra of RhB solution degraded by CFe1 (**a**), CFe2 (**b**), CFe3 (**c**) and the comparison of the degradation of RhB by CFe1, CFe2, CFe3 (**d**)

4 Conclusions

In general, the modified pomelo peel biochar composites with iron ion are efficient for the adsorption and photocatalysis of organic pollutants, the final capacities of the 3 biochar composites after 105 min are almost equal and reach around 90% degradation of RhB. The biochar composites obtained via hydrothermal treatment have stronger adsorption performances with larger specific surface areas and more uniform pore sizes than the calcined one, however, the calcined biochar composite has a better photocatalytic performance due to the existence of α-Fe_2O_3. The effect of the cycle test is not satisfying, but CFe2 is more stable than CFe1. By comparing the results of CFe1 on RhB and imidacloprid, we find that CFe1 is selective for adsorption and photocatalysis of different pollutants.

More researches are ongoing. On the one hand, to study how to enhance the stability of biochar composites so that there is no much loss in the cycle test. On the other hand, we continue to study the modification and activation of biochar materials and hope to improve the removal of pesticide wastewater by the low cost biochar materials in the near future.

Acknowledgements Authors acknowledge the support by NSFC Project 21571132, by the Open Fund (RERU2017005) of National Key Laboratory of Rare Earth Resources Utilization, and by the key Project (LZGD2017002) of Department of Education of Liaoning Province. This work is also supported by College Students Innovation and Entrepreneurship Competition, Shenyang University of Technology.

Compliance with ethical standards

Conflict of interest The authors declare that they have no conflict of interests.

References

1. An F, Feng X, Gao B (2009) Adsorption of aniline from aqueous solution using novel adsorbent PAM/SiO_2. Chem Eng J 151(1–3):183–187
2. Najafi M, Yousefi Y, Rafati AA (2012) Synthesis, characterization and adsorption studies of several heavy metal ions on amino-functionalized silica nano hollow sphere and silica gel. Sep Purif Technol 85:193–205
3. Batzias F, Sidiras D (2004) Dye adsorption by calcium chloride treated beech sawdust in batch and fixed-bed systems. J Hazard Mater 114(1):167–174
4. Zhao XR, Qin ZF, Yang ZZ, Zhao Q, Zhao YX, Qin XF, Zhang YC, Ruan XL, Zhang YF, Xu XB (2010) Dual body burdens of polychlorinated biphenyls and polybrominated diphenyl ethers among local residents in an e-waste recycling region in Southeast China. Chemosphere 78(6):659–666
5. Jana M, Sil A, Ray S (2012) Influence of melting of transition metal oxides on the morphology of carbon nanostructures. Adv Mater Res 585:159–163
6. Wang XY, Shang W (2002) Hazards of toxic organic pollutants in water and priority control of pollutants. J Capital Normal Univ 23(3):73–76
7. Malik DJ (2005) Interpretation of transition metal sorption behavior by oxidized active carbons and other adsorbents. Sep Sci Technol 39(8):1885–1905
8. Hasan Z, Jhung SH (2015) Removal of hazardous organics from water using metal-organic frameworks (MOFs): plausible mechanisms for selective adsorptions. J Hazard Mater 283:329–339
9. Khan E, Li MH, Huang CP (2007) Hazardous waste treatment technologies. Water Environ Res 79(10):1858–1902
10. Zhou Y, Xiao B, Liu SQ, Meng Z, Chen ZG, Zou CY, Liu CB, Chen F, Zhou X (2015) Photo-fenton degradation of ammonia via a manganese–iron double-active component catalyst of graphene–manganese ferrite under visible light. Chem Eng J 283(12):266–275
11. Ruan C-P, Ai K-L, Lu L-H (2016) An acid-resistant magnetic Co/C nanocomposite for adsorption and separation of organic contaminants from water. Chin J Anal Chem 44(2):224–231
12. Bakhtiari N, Azizian S, Alshehri SM, Torad NL, Malgras V, Yamauchi Y (2015) Study on adsorption of copper ion from aqueous solution by MOF-derived nanoporous carbon. Microporous Mesoporous Mater 217:173–177
13. Aksu Z (2005) Application of biosorption for the removal of organic pollutants: a review. Process Biochem 40(3–4):997–1026
14. Chen B, Yuan M, Liu H (2011) Removal of polycyclic aromatic hydrocarbons from aqueous solution using plant residue materials as a biosorbent. J Hazard Mater 188(1–3):436–442
15. Mohan D, Sarswat A, Ok YS, Pittman CU (2014) Organic and inorganic contaminants removal from water with biochar, a renewable, low cost and sustainable adsorbent—a critical review. Bioresour Technol 160:191–202
16. Xiao G, Long L (2012) Efficient removal of aniline by a water-compatible microporous and mesoporous hyper-cross-linked resin and XAD-4 resin: a comparative study. Appl Surf Sci 258(17):6465–6471
17. Ferrero F (2007) Dye removal by low cost adsorbents: hazelnut shells in comparison with wood sawdust. J Hazard Mater 142:144–152
18. Garg VK, Gupta R, Yadav AB, Kumar R (2003) Dye removal from aqueous solution by adsorption on treated sawdust. Bioresour Technol 89:121–124
19. Garg VK, Kumar R, Gupta R (2004) Removal of malachite green dye from aqueous solution by adsorption using agro-industry waste: a case study of *Prosopis cineraria*. Dyes Pigments 62:1–10
20. Zhang RZ (2015) Preparation of the functional modified pine sawdust and its adsorption/photocatalytic performance. East China University of Science and Technology, pp 5–7
21. Chen L, Bai B (2013) Equilibrium, kinetic, thermodynamic, and in situ regeneration studies about methylene blue adsorption by the raspberry-like TiO_2@yeast microspheres. Ind Eng Chem Res 52(44):15568–15577
22. Wang G, Qi P, Xue X, Wu F, Deng N (2007) Photodegradation of bisphenol Z by UV irradiation in the presence of β-cyclodextrin. Chemosphere 67(4):762–769
23. Mohapatra L, Parida K, Satpathy M (2012) Molybdate/tungstate intercalated oxo-bridged Zn/Y LDH for solar light induced photodegradation of organic pollutants. J Phys Chem C 116:13063–13070
24. Han F, Kambala VSR, Srinivasan M, Rajarathnam D, Naidu R (2009) Tailored titanium dioxide photocatalysts for the degradation of organic dyes in wastewater treatment: a review. Appl Catal A Gen 359(1):25–40
25. Singh R, Dutta S (2018) A review on H_2 production through photocatalytic reactions using TiO_2/TiO_2-assisted catalysts. Fuel 220:607–620
26. Kumar SG, Devi LG (2011) Review on modified TiO_2 photocatalysis under UV/visible light: selected results and related mechanisms on interfacial charge carrier transfer dynamics. J Phys Chem A 115(46):13211–13241
27. Xie LJ, Ma JF, Zhao ZQ, Tian H, Zhou J (2005) Research status and prospects of semiconductor photocatalysts. Bull Chin Ceram Soc 6:80–84
28. Khan SUM, Alshahry M, Ingler WBJ (2002) Efficient photochemical water splitting by a chemically modified n-TiO_2. Science 297(5590):2243–2245
29. Azargohar R, Dalai A (2008) Steam and KOH activation of biochar: experimental and modeling studies. Microporous Mesoporous Mater 110(2):413–421
30. Qian K, Kumar A, Zhang H, Bellmer D, Huhnke R (2015) Recent advances in utilization of biochar. Renew Sustain Energy Rev 42:1055–1064
31. Alker JD, Tannenbaum R (2006) Characterization of the sol–gel formation of iron(III) oxide/hydroxide nanonetworks from weak base molecules. Chem Mater 18:4793–4801
32. Wang DB, Song CX, Zhao YH, Yang ML (2008) Synthesis and characterization of monodisperse iron oxides microspheres. J Phys Chem C 112:12710–12715
33. Mu J, Liu D-X, Bai Y, Yao Q, Qian F, Shi F-N (2018) Pomelo peel biochar design and the adsorption and photocatalytic properties. Adv Eng Res 174:31–36